doi:10.1038/nature14861

Systematic shift caused by trap asymmetry

The major systematic correction in the reported cyclotron frequency ratio comparison of an antiproton at $\nu_{c,\bar{p}}$ and a negatively charged hydrogen ion (H^-) at ν_{c,H^-} is caused by a spatial shift Δz of the different particle species in a magnetic gradient B_1 caused by a magnetic electrode which will be used for planned antiproton magnetic moment measurements. The spatial shift Δz is caused by the adjustment of the trapping voltage to tune both trapped particles to resonance with the axial detection system at $\nu_{\mathrm{res}} = 645\,262\,\mathrm{Hz}$.

The axial frequency ν_z of a particle with charge-to-mass ratio q/m in a Penning trap is given by

$$\nu_z = \frac{1}{2\pi}\sqrt{\frac{2C_2 q V_R}{m}}\,, \tag{1}$$

where V_R is the voltage applied to the trap electrodes and $1/\sqrt{C_2}$ is a trap specific length, in our case $C_2 = 18404\,\mathrm{m}^{-2}$. Thus, the voltage to tune an antiproton to resonance with the detector is $V_{R,\bar{\mathrm{p}}} = 4.662035\,\mathrm{V}$, and the difference which is required to adjust the axial frequencies of the H^- ion ν_{z,H^-} to ν_{res} is $(V_{R,\mathrm{H}^-} - V_{R,\bar{\mathrm{p}}}) = \Delta V_R = 0.005003\,\mathrm{V}$.

In case of a perfectly symmetric trap the voltage adjustment does not affect the particle position. However, machining errors, mounting tolerances, and offset potentials ΔV_k, which are present on the individual trap electrodes, in the further discussion partly replaced by the term "trap asymmetry", contribute to a shift $\Delta z(\Delta V_R)$. The magnitude of this shift can be characterized by performing adequate systematic measurements.

Trap geometry. – The geometry of our trap is shown in Fig. 1. It consists of five electrodes,

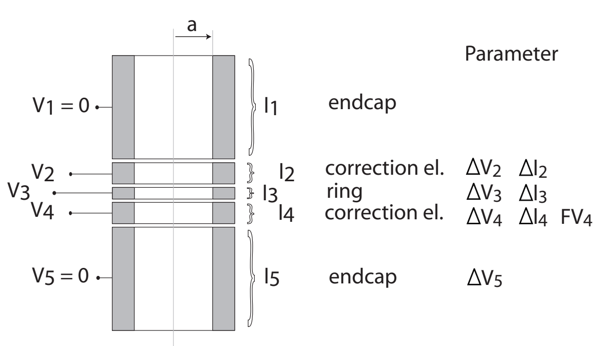

FIG. 1. Cylindrical Penning trap in orthogonal, compensated design. For details, see text.

which are two endcap electrodes, one ring electrode and two correction electrodes adjacent to the ring. The two correction electrodes are used to compensate higher order coefficients C_4 and C_6 of the electrostatic potential [1].

- The trap geometry is chosen in a way that the higher order potential coefficients $C_4(\mathrm{TR})$ and $C_6(\mathrm{TR})$ simultaneously vanish for a certain tuning ratio $\mathrm{TR} = V_{2,4}/V_3$, which is the ratio of the voltage $V_{2,4}$ applied to the correction electrodes and the voltage V_3 applied to the ring. This feature is called "compensation".

- The trap parameter $C_2 = E_2 + D_2 \cdot \mathrm{TR}$, where E_2 is a trap specific constant and D_2 is called "orthogonality". The trap lengths are chosen in a way that $D_2 = 0$, and thus C_2 is independent of the tuning ratio.

This geometry results from a careful design procedure described in [2].

In our case the diameter of the trap is $2a = 9\,\mathrm{mm}$, the lengths l_1 and l_5 of the endcaps are $> 30\,\mathrm{mm}$ and can be considered as infinite, the ring electrode has a length of $l_3 = 1.13\,\mathrm{mm}$ and the correction electrodes are $l_2 = l_4 = 3.53\,\mathrm{mm}$. The electrodes are spaced by sapphire rings, the inner distance between adjacent electrodes is $d = 0.14\,\mathrm{mm}$.

Analytical solutions are used to calculate the trapping potential. The potential $\phi_k(z, l_k, V_k)$ of electrode k is described by a series

$$\phi_k(z, l_k, V_k) = V_k \cdot \sum_{n=1}^{\infty} \frac{f(m_n, l_k, z)}{I_0(m_n a_k)}\,, \tag{2}$$

with diameter $2 \cdot a_k$ of the individual electrode. Here $I_0(m_n a_k)$ is the modified Bessel function of second kind and zeroth order, $f(m_n, l_k, z)$ are trigonometric functions, and $m_n = n\pi/L$, where L is the length of the trap. Within deviations on the percent-level of the trap diameter any geometric modification Δl_k in electrode length can be locally compensated by an appropriate adjustment of the trap diameter $2 \cdot a_k \to 2 \cdot (a_k + \Delta a_k)$ to keep

$$V_k \sum_{n=1}^{\infty} \frac{f(l_k, z)}{I_0(a_k)} = V_k \sum_{n=1}^{\infty} \frac{f(l_k + \Delta l_k, z)}{I_0(a_k + \Delta a_k)} \tag{3}$$

constant within error bars. The machining precision of the diameter of our trap is $\leq 5\,\mu\mathrm{m}$, which corresponds to a relative modification of the diameter by $0.056\,\%$, thus we keep in the following discussion $2 \cdot a_k = 9\,\mathrm{mm}$ constant.

The trap asymmetry consisting of offset voltages ΔV_k applied to the electrodes as well as geometric errors Δl_k and tiny voltage dividers F_k due to current leaks in the trap wiring have to be determined. Here we define that the voltage applied to trap electrode k is $F_k \cdot V_k$, where V_k is the voltage applied at the output of our power-supply. Since the endcaps can be considered as infinitely long we set $\Delta l_1 = \Delta l_5 = 0$. From leakage current measurements $F_k > 0.998$ is extracted being negligibly small except for F_4, which has to be extracted by measurement. At this electrode the single particle detector is placed and a current leak is present at the DC-biasing network. Thus the parameters ΔV_k, Δl_2, Δl_3, Δl_4 and F_4 have to be determined.

Voltage divider. – In order to measure the magnitude of the voltage divider F_4 we use particle separation [3]. A cloud of particles is stored in the center of the trap and a voltage ramp applied to the central trap electrode is used to separate the particles into two fractions. Afterwards we count the particles extracted to the upstream- and the downstream-side of

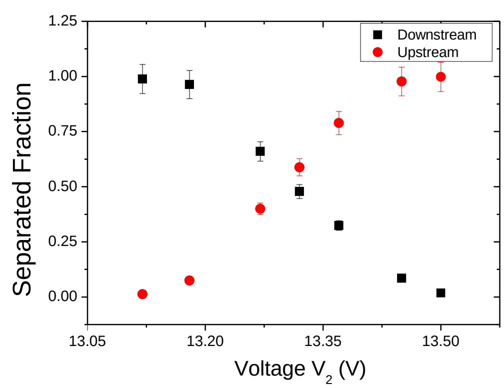

FIG. 2. Fraction of particles extracted to downstream- (black squares) and upstream- (red circles) side of the trap by using separation ramps. From this measurement we determine the voltage divider $F_4 = 0.985(2)$ present on trap electrode 4. Error bars are due to the uncertainties in the fits of the used particle-dips [3].

the trap by recording dip spectra and fitting the widths of the many-particle dips, which is proportional to the number of trapped particles. The number of particles has to be identical for symmetric conditions. Results of such a measurement are shown in Fig. 2 and allow the determination of F_4 with an absolute uncertainty of 0.002. Using the correction voltages extracted below we find $F_4 = 0.985(2)$.

doi:10.1038/nature14861

Offset Voltages and Geometric Offsets. – To determine the offset voltages and geometric offsets, we measure:

- the voltages which tune the axial oscillation frequencies ν_z of the particles to resonance with the axial resonator at ν_{res} as a function of voltages δV_k which are deliberately applied to the correction electrodes. Thus we obtain data-sets $V_R(\delta V_k)$ and eventually $C_2(\delta V_k)$.
- For each offset δV_k we optimize the tuning ratio and obtain data-sets $\mathrm{TR}_{\mathrm{opt}}(\delta V_k)$, for some parameters we determine the compensation $C_4(\mathrm{TR})$ and $C_6(\mathrm{TR})$.

These measurements are performed for offsets applied to the downstream correction electrode (δV_2) as well as to the upstream correction electrode (δV_4). In addition we compare

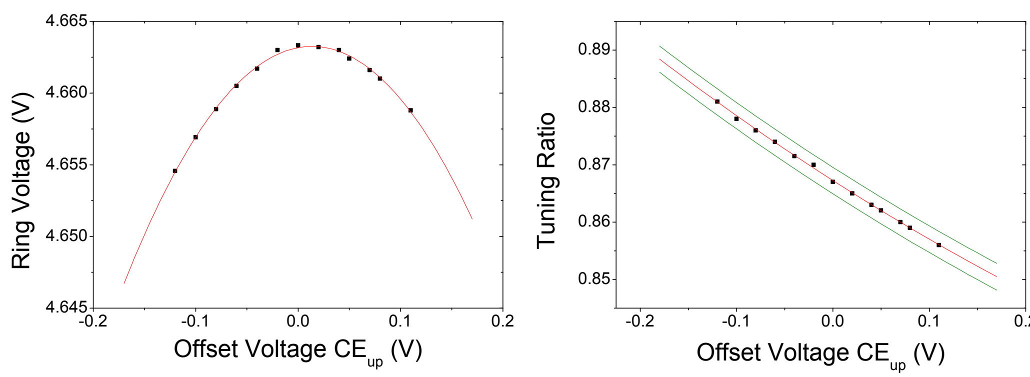

FIG. 3. Left panel: Measurements $C_2(\delta V_4)$ (red solid circles) and fit of potential theory to the data. This fit gives values ΔV_4 and ΔV_5 for the free parameters ΔV_1, ΔV_2 and ΔV_3. Right panel: Measured $\mathrm{TR}(\delta V_2)$ (red points) and fits of potential theory to the data (solid lines). These data-sets define $\Delta V_3(\Delta V_1, \Delta V_2)$. The green lines are results from potential theory with the fitted value $\Delta V_3 \pm 10\,\mathrm{mV}$, which depicts the scaling. Error bars are on the scale of the point-size of the data representation.

to data-sets measured with protons and switched polarity.

The data sets $C_2(\delta V_k)$ enable the determination of the voltage offsets ΔV_4 and ΔV_5 with the remaining voltages as free parameters. The data-set $\mathrm{TR}_{\mathrm{opt}}(\delta V_k)$ enables extraction of $\Delta V_3(\Delta V_1, \Delta V_2)$. Figure 3 shows fits of potential calculations to the measured data. The left panel represents measurements $C_2(\delta V_4)$ (black solid squares) and a fit of potential theory to the data, which gives values ΔV_4 and ΔV_5 for the remaining voltages as free parameters. The uncertainty of the fit parameters is $\Delta V_{4,f} \approx 1\,\mathrm{mV}$ and for $\Delta V_{5,f} \approx 2\,\mathrm{mV}$, respectively. The right panel shows measured $\mathrm{TR}(\delta V_4)$ (black squares) and fits of potential theory to the data. These data-sets define $\Delta V_3(\Delta V_1, \Delta V_2)$. The green lines are results from potential theory with the fitted value $\Delta V_3 \pm 10\,\mathrm{mV}$ for constant ΔV_1 and ΔV_2. Eventually the measured data-sets $D_2(\delta V_k)$ and comparisons to measurements carried-out with protons allow us to determine ΔV_1 and ΔV_2. Figure 4 shows results of the parameter D_2 as a function of the offset voltage δV_2. The red solid circles are measured data, the error-bars are at the level of 0.1 % and not visible. The blue line is a fit based on potential theory yielding the applied offset-voltage ΔV_2, the green lines are fits for potential offsets with $\Delta V_2 \pm 30\,\mathrm{mV}$. Based on the measured data we are able to determine ΔV_1 and ΔV_2 with uncertainties of 9 mV and 5 mV, respectively. In addition to the determination of the offset voltage ΔV_2

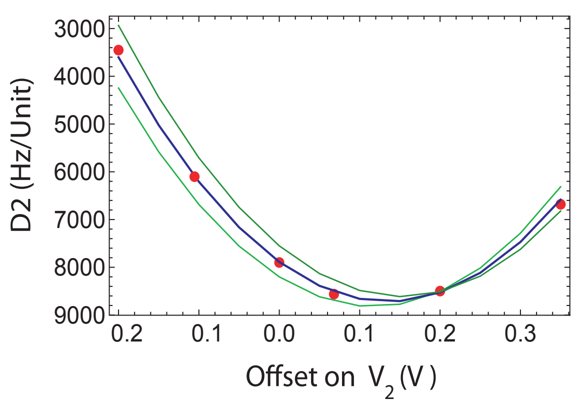

FIG. 4. Measurement of D_2 (red solid circles) in Hz/Unit as a function of the offset voltage δV_2 which is deliberately applied to electrode 2. Error bars are on the scale of the point-size of the data representation. For details see text.

the measurement of the parameter $D_2(\delta V_k)$ enables us to extract the geometric offsets. In the ideal, symmetric case D_2 is ≥ 0, having a minimum close to the exact compensation of the offset voltages since the voltages V_k and geometric offsets Δl_k factorize. Moreover, $dD_2/dl_3 < 0$ and $dD_2/dl_2 = dD_2/dl_4 < 0$. A length modification Δl_3 leads to a shift of the minimum of the $D_2(\delta V_k)$ parabola, but keeps it symmetric. The offsets Δl_2 and Δl_4 add an asymmetry to $D_2(\delta V_k)$. In order to fix the offsets Δl_2, Δl_3 and Δl_4 we fit the measurements $D_2(\delta V_2)$ and $D_2(\delta V_4)$. The offset ΔV_1 is obtained from the measurements

$D_2(\delta V_2)$ and $D_2(\delta V_4)$ as well as the proton measurements. By iterative application of the formalism describing the qualitative behaviour summarized above, and counting the offset extracted as ΔV_4 to correct F_4, the offsets which are present on the trap are obtained. A manuscript describing the details of this analysis is in preparation.
The offsets obtained from this data evaluation are listed in Tab. I. By using these offsets and switching the polarity from protons to antiprotons we reproduce the resonance voltage $V_{3,p}$ to tune the proton to $\nu_{z,0}$ with an uncertainty of 0.3 mV as well as the ideal tuning ratio TR_p for protons with a relative accuracy of 0.1 %. Our extracted parameters are as well consistent with compensation measurements $C_4(\mathrm{TR})$ and $C_6(\mathrm{TR})$.

Magnetic Field Measurement. – By applying offset voltages δV_2 and δV_4 the position $z_0(\delta V_k) = C_1(\delta V_k)/(2C_2(\delta V_k))$ of the particle in the trap can be shifted. This allows for a measurement of the cyclotron frequency and thus the magnetic field as a function of particle position $z_0(\delta V_k)$. We fit to these $\nu_c(z_0(\delta V_k)) \propto B(z_0(\delta V_k))$ data second order polynomials $B_0 + B_1 z_0 + B_2 z_0^2$ and obtain the parameters

$$B_{1,exp} = -0.00758(42)\,\mathrm{T/m} \tag{4}$$

$$B_{2,exp} = 0.0068(91)\,\mathrm{T/m^2}\,. \tag{5}$$

Both parameters were measured frequently to confirm their temporal stability, specifically of the crucial gradient term B_1.

Shift of the Measured Charge-to-Mass Ratio induced by Trap Asymmetry. – The above trap asymmetry and the measured B_1-value enable the calculation of the systematic shift in the measured cyclotron frequency ratio by

$$\left(\frac{\Delta R}{R}\right)_{\mathrm{as}} = \frac{B_1 \Delta z(\Delta V_R)}{B_0}. \tag{6}$$

Table I summarizes the error of the equivalent ratio correction due to the uncertainties in the determined offset voltages. By inserting the offsets shown in Tab. I we obtain a ratio correction of $-114(26)$ p.p.t..

Ratio Shift induced by the Octupolar Potential Correction. – We optimize the tuning ratio of our trap by measuring the axial frequency of the antiproton as a function of the

TABLE I. Offset voltages, geometric offsets and voltage divider present on electrode 4 (See Fig. 1).

parameter	value	uncertainty	uncertainty in ratio shift in p.p.t.
ΔV_1	0 mV	9 mV	9.9
ΔV_2	−2 mV	5 mV	12.4
ΔV_3	0 mV	7 mV	0.2
ΔV_4	119 mV	1 mV	2.5
ΔV_5	−10 mV	2 mV	2.2
Δl_2	18 μm	4 μm	4.7
Δl_3	29 μm	1 μm	1.1
Δl_4	0 μm	4 μm	4.7
F_4	0.985	0.002	19.8

magnetron radius and for different tuning ratios. From these measurements we obtain values $C_4(\mathrm{TR})$, a linear fit allows for optimization of the tuning ratio with $\delta\mathrm{TR}/\mathrm{TR} = 5 \cdot 10^{-6}$, to set $C_4(\mathrm{TR}_{\mathrm{opt}} = 0)$. However, in presence of the trap-offsets discussed above, the adjustment of the trapping voltage by ΔV_R shifts the effective C_4 coefficients seen by the H^- ion by $\Delta\mathrm{TR} = 0.000022$. This contributes an effective shift of the cyclotron frequency $\Delta\nu_c/\nu_c \propto f(C_4, E_+, E_z)$ [1], where E_+ and E_z have to be determined by measurement.

During frequency measurements the particles are in thermal contact with the axial detection system, which thus defines the axial energy $E_z/k_B = T_z$ of the particle, where k_B is the Boltzmann-constant. The resonance frequency of the axial detector is 645262 Hz. The device has a quality factor of 11300 and an inductance of 1.72 mH. This corresponds to an effective parallel resistance of $R_P = 78.5\,\mathrm{M\Omega}$. The signal-to-noise ratio of the detector is at 31 dB. Together with the effective pickup-length of 10.06 mm we obtain a cooling time constant of $\tau_{RT} = 83\,\mathrm{ms}$, which corresponds to a dip-width of 1.90 Hz. From measurements we extract 1.91(16) Hz.

From signal-to-noise ratio measurements and independent measurements of the equivalent input-noise e_n of the amplifier and the coupling factor κ from the resonator to the amplifier we obtain information about the temperature of the detector

$$T_z = 5.2(1.1)\,\mathrm{K}\,. \tag{7}$$

Another approach to determine the axial temperature of the particle is based on the cloud separation described above (see Fig. 2) and as well in [3]. The fraction extracted to the upstream and the downstream side of the trap as a function of a deliberately applied trap asymmetry scales sensitively with particle temperature. From this evaluation we obtain

$$T_z = 5.5(1.5)\,\mathrm{K}\,, \tag{8}$$

which is in agreement with the value extracted in Eqn. (7). The resulting cyclotron energy $E_+/k_B = T_+$ in a sideband measurement is thus

$$T_+ = \frac{\nu_+}{\nu_z} T_z = 243(49)\,\mathrm{K}\,. \tag{9}$$

With these temperatures and the effective tuning ratio change quoted above the contributed shift of the cyclotron frequency is at

$$\frac{\Delta\nu_{c,\mathrm{H}^-}}{\nu_{c,\mathrm{H}^-}} = -0.6(1)\,\mathrm{p.p.t./K}\cdot\mathrm{T}_z, \tag{10}$$

and with the axial temperature measurement above we obtain a fractional ratio shift of

$$\left(\frac{\Delta R}{R}\right)_{C_4} = -3(1)\,\mathrm{p.p.t.}. \tag{11}$$

Drifts of the voltage source – The above discussion assumes that the voltage source can be considered as “infinitely” stable. Each channel which is used to bias one of the correction electrodes or the ring electrode has a stability of $\Delta V/V \approx 10^{-7}$/cycle. During the precision frequency measurements the endcaps are switched to ground.

Each electrode is biased by RC-filters with a total time constant of 20 ms. Additional time constants due to parasitic relaxation of capacitor dielectrics are < 1.6 s. After the initial 10 s cooling of the magnetron motion the voltage reproducibility between subsequent measurement cycles is at the trap operation voltage of 4.6 V at ≈ 500 nV, producing negligible systematic shifts caused by voltage drifts and thus induced shifts Δz.

Additional systematic shifts can be caused by voltage drifts which shift the axial frequency between the sideband measurement and the determination of ν_z. From the entire sequence of axial frequency measurements the average voltage drift per cyclotron frequency measurement can be extracted, which is in units of frequency at $\Delta\nu_z = -0.69(15)$ mHz. The ratio shift which is induced by this drift is given as

$$\left(\frac{\Delta R}{R}\right)_{\mathrm{V}} \approx \frac{\Delta\nu_z}{\nu_{c,\bar{p},\mathrm{H}^-}}\,(1-R) \approx 0.015(3)\,\mathrm{p.p.t.}\,. \tag{12}$$

TABLE II. Summary of ratio shifts which contribute on the sub-p.p.t. level.

Effect	Shift (p.p.t.)	Uncertainty (p.p.t.)
Magnetic gradient shift	-0.002	0.0002
Magnetic bottle shift	0.009	0.012
Image charge shift	0.047	0.004
Image current shift	<| 0.001 |	<| 0.001 |
Relativistic shift	-0.024	0.002
Voltage drift	0.015	0.003
Tilt of apparatus	-0.027	0.007
Rb-clock	–	3

Tilt of apparatus – As discussed in the main article, the magnetron frequency is determined by using the ideal relation $\nu_- = \nu_z^2/(2\nu_+)$. A tilt of the electrostatic trap axis with respect to the magnetic field axis shifts the magnetron frequency to $\nu_- = 9/4 \cdot \nu_z^2/(2\nu_+) \cdot \sin^2(\theta)$, where θ is the angle between the magnetic and the electrostatic axis. This angle can be determined by measuring the magnetron frequency explicitly using the sideband method. From experiments we find $\theta = 0.4(1)$ degrees. The error in the ratio caused by this angle can be rewritten

$$\left(\frac{\Delta R}{R}\right)_\theta \approx \frac{9}{16} \sin^2(\theta) \left(\frac{\nu_z^4}{\nu_+^4}\right) \left(1 - R^4\right) \approx -0.027(7)\,\text{p.p.t.}\,. \tag{13}$$

Additional frequency shifts

Cyclotron frequency shifts induced by magnetic inhomogeneities which are traced by the finite thermal particle energies, as well as relativistic shifts, image charge shift and shifts induced by detector damping are on the sub-p.p.t. level [1]. In addition to these standard shifts the stability of the used Rb clock contributes an uncertainty of 3 p.p.t.. For completeness these shifts are summarized in Tab. II.

[1] Brown, L. S. & Gabrielse, G. Geonium theory: physics of a single electron or ion in a Penning trap. *Rev. Mod. Phys.* **58**, 233311 (1986).

[2] Gabrielse, G., Haarsma, L. & Rolston L. S. Open-endcap Penning traps for high precision experiments. *Int. J. Mass Spec.* **88**, 319-324 (1989).

[3] Smorra, C. *et al.*, A reservoir trap for antiprotons, submitted (2015).

[4] Smorra, C. *et al.*, Towards a high-precision measurement of the antiproton magnetic moment. *Hyperfine Interact.* doi:10.1007/s10751-014-1018-7 (2014).

[5] Ulmer, S. *et al.*, The quality factor of a superconducting resonator in a magnetic field. *Rev. Sci. Inst.* **80**, 123302 (2009).

[6] Brown, L. S. & Gabrielse, G. Precision spectroscopy of a charged particle in an imperfect Penning trap. *Phys. Rev. A* **25**, 2423-2426 (1982).